Ultrasound in Med. & Biol., Vol. 37, No. 9, pp. 1500–1508, 2011

0301-5629/$ - see front matter

ELSEVIER

doi:10.1016/j.ultrasmedbio.2011.05.025

● *Original Contribution*

DYNAMICS OF COATED MICROBUBBLES ADHERENT TO A WALL

Marlies Overvelde,* Valeria Garbin,*[1] Benjamin Dollet,† Nico de Jong,*‡
Detlef Lohse,* and Michel Versluis*

*Physics of Fluids Group, Research Institute for Biomedical Technology and Technical Medicine MIRA, University of Twente, Enschede, The Netherlands; †Institut de Physique de Rennes, UMR 6251 CNRS/Université Rennes 1, Rennes, France; and ‡Biomedical Engineering, Erasmus MC, Rotterdam, The Netherlands

(*Received* 25 *August* 2010; *revised* 18 *May* 2011; *in final form* 20 *May* 2011)

Abstract—Molecular imaging with ultrasound is a promising noninvasive technique for disease-specific imaging, enabling for instance, the diagnosis of thrombus and inflammation. Selective imaging is performed by using ultrasound contrast agent microbubbles functionalized with ligands, which bind specifically to the target molecules. Here, we investigate in a model system, the influence of adherence at a wall on the dynamics of the microbubbles, in particular, on the frequency of maximum response, by recording the radial response of individual microbubbles as a function of the applied acoustic pressure and frequency. The frequency of maximum response of adherent microbubbles was found to be over 50% lower than for bubbles in the unbounded fluid and over 30% lower than that of a nonadherent bubble in contact with the wall. The change is caused by adhesion of the bubbles to the wall as no influence was found due solely to the presence of the targeting ligands on the bubble dynamics. The shift in the frequency of maximum response may prove to be important for molecular imaging with ultrasound as this application would benefit from an acoustic imaging method to distinguish adherent microbubbles from freely circulating microbubbles. (E-mail: m.versluis@utwente.nl) © **2011 World Federation for Ultrasound in Medicine & Biology.**

Key Words: **Ultrasound contrast agents, Microbubbles, Targeting, Adherent, Nonlinear bubble dynamics, Resonance, Ligands, Molecular imaging.**

INTRODUCTION

The use of contrast agents in medical imaging with ultrasound is well established. The contrast agent is injected intravenously and is designed to enhance the contrast of the blood pool. The most common ultrasound contrast agent (UCA) is composed of a suspension of microbubbles (radius 0.5–5 μm), which are coated with a phospholipid, albumin or polymer shell. The coating reduces the surface tension σ and, therefore, the capillary pressure $2\sigma/R$. Moreover, the coating increases the diffusive timescales and the combined effect prevents the bubble from quickly dissolving in the blood.

A promising application is noninvasive molecular imaging for selective diagnosis with ultrasound using contrast agent microbubbles. Targeting ligands are incorporated in the coating of ultrasound contrast agent microbubbles to selectively bind to biomarkers on the membrane of endothelial cells, which constitute the blood vessel wall. A series of challenges are encountered in the development of targeted microbubbles for molecular imaging applications.

The first question, as was stated by Lindner (2004), is whether bubbles adhering to a target cell produce strong enough acoustic signals. It was found that the response of adherent microbubbles is comparable to that of phospholipid-coated microbubbles (Zhao et al. 2006; Lankford et al. 2006). However, it remains to be seen if the concentration of adherent microbubbles *in vivo* will be high enough to produce signals in the order of normal contrast-enhanced ultrasound in perfusion imaging.

Another challenge that has received significant attention is the adhesion of the bubbles to the vessel wall under shear flow. Primary radiation force has been used to effectively push the bubbles towards the vessel (Dayton et al. 1999, 2002; Takalkar et al. 2004; Rychak et al. 2007; Zhang et al. 2007; Doinikov et al. 2009).

Address correspondence to: Michel Versluis, Physics of Fluids Group, Research Institute for Biomedical Technology and Technical Medicine MIRA, P.O. Box 217, 7500 AE Enschede, The Netherlands. E-mail: m.versluis@utwente.nl

[1]Present address: Department of Chemical and Biomolecular Engineering, University of Pennsylvania, 220 South 33rd Street, Philadelphia PA 19104, USA.

Engineering of the ligands has led to a method to increase the number of adherent microbubbles. The use of two distinct antibody-receptor pairs has been proposed (Eniola et al. 2003), as well as the use of a polymeric version of the ligand to increase the ligand surface density (Klibanov et al. 2006; Klibanov 2009) and the use of a longer spacer arm (Ham et al. 2009).

Finally, one should be able to distinguish adherent microbubbles from freely circulating ones (Lindner 2004). The simplest approach is to wash out all the freely circulating microbubbles and image the remaining bubbles. The disadvantage is that it takes 5 to 10 min before all freely circulating bubbles are cleared by the liver and spleen and that there is no new supply of bubbles. Therefore, it would be beneficial to distinguish acoustically between adherent and freely circulating microbubbles. Considerable changes between adherent and nonadherent microbubbles were found, such as a change in the spectral response (Zhao et al. 2006) and a decrease in the acoustic response of adherent microbubbles with respect to nonadherent ones (Lankford et al. 2006).

Garbin et al. (2007) showed for one and the same bubble that the close proximity of a wall decreased the radial amplitude of oscillation by 50%. *In vivo* the bubbles circulate freely in the blood vessel and their position with respect to the wall is unknown. A change in the dynamics of a bubble solely due to the proximity of the boundary is, therefore, not sufficient to differentiate between freely circulating bubbles and adherent bubbles. Consequently, it is important to understand the influence of adherence to a wall on the bubble dynamics. Furthermore, we would like to investigate under what conditions the response of adherent and freely circulating bubbles can be differentiated, to optimize them for pulse-echo techniques.

Here, we investigate the change in the dynamics of adherent microbubbles with respect to bubbles in the unbounded fluid. In the Methods section, we describe the set-up, experimental methods and the preparation of the bubbles. The influence of targeting ligands, the proximity of the wall and the adhesion to the wall on the frequency of maximum response and the amplitude of oscillation will be shown in the Results section. In the Discussion section, we discuss the results and conclude.

METHODS

Set-up

An OptiCell chamber (Thermo Fisher Scientific, Waltham, MA, USA) containing the contrast agent was positioned in a water tank. The custom designed water tank held the illumination fiber and the ultrasound transducer (PA168; Precision Acoustics, Dorchester, United Kingdom). The acoustic driving pulse was generated by an arbitrary waveform generator (Tabor 8026; Tabor Electronics, Tel Hanan, Israel). The pulse consisted of a burst of 10 cycles where the first and last three cycles were tapered with a cosine window. We based the choice for this specific pulse on the following. First, we minimize transient effects by tapering the first and last three cycles with a cosine window. Furthermore, the amplitude of oscillation is determined from a set of stable oscillations. And finally, the length of the pulse is minimized to avoid shrinkage of the bubble. The total pulse length should then fit within the acquisition time of the camera. The pulse was amplified by an RF-amplifier (ENI 350L; Electronic Navigation Industries, Inc., Rochester, NY, USA). Imaging of the sample was performed through a microscope equipped with a water-immersed 100 $\times$ objective (LUMFPL; Olympus, Zoeterwoude, The Netherlands). The microscope was connected to a set-up combining the ultra-high speed camera Brandaris 128 (Chin et al. 2003) and optical tweezers, described in detail by Garbin et al. (2007). The radial dynamics was captured at a framerate of 14 million frames per second (Mfps).

The transducer was calibrated in the frequency range from 0.75 MHz to 5.0 MHz. The sensitivity of the transducer at frequencies below 1.2 MHz is limited and only very low pressures could be generated below this frequency. We repeated the experiment multiple times on the very same bubble for increasing acoustic pressure, see for a detailed explanation on the set-up and protocol Overvelde et al. (2010b). The transducer was calibrated prior to the experiments with a 0.2 mm needle hydrophone (HPM02/1; Precision Acoustics, Dorchester, United Kingdom). The center frequency of the hydrophone is 3.5 MHz and was calibrated by Precision Acoustics between 0.5 and 10 MHz. The acoustic focus of the transducer and the optical focus of the microscope objective were aligned as follows: the OptiCell was removed, the tip of the hydrophone was positioned in the focus of the microscope objective with a XYZ-micropositioning stage and the transducer was aligned with a planar-stage. To keep the optical and acoustical focus aligned, the OptiCell chamber was connected to a three-dimensional (3-D) stage to allow for the movement of the sample independently of the transducer and the microscope.

Preparation

BG-6437 and BG-6438 (Bracco Research S.A., Geneva, Switzerland) are gas microbubbles of approximately 3 μm in diameter, containing a mixture of perfluorobutane and nitrogen stabilized by a lipid envelope. These agents are prepared according to a procedure described by Schneider et al. (1991) and a microbubble suspension is obtained by dispersing the lyophilized product in 1 mL

saline solution. The components of the coated microbubbles have been selected on the basis of their ability to generate stable bubbles and good imaging performance over a broad range of frequencies (2–10 MHz). BG-6438 in addition contains streptavidin molecules chemically incorporated onto the lipid shell (approx. 3000/μm^2), to allow functionalization of the gas microbubbles with biotin-conjugated ligands.

The experimental contrast agents BG-6437 and BG-6438 were prepared following the protocols described below. The BG-6437 bubbles were prepared by injecting 1 mL of sterile saline (0.9% sodium chloride; B. Braun Medical Ltd., Sheffield, United Kingdom) through the rubber stopper of the vial, while a second needle was used for venting the excess pressure. The vial was shaken for 5–10 s and the suspension was left to rest for 5 min. The BG-6438 microbubbles were reconstituted following the same protocol described above with the difference that 0.7 mL of sterile saline was injected. A polyclonal anti-fluorescein antibody (200-1996; Rockland, Gilbertsville, PA, USA) was biotinylated using the kit and protocol of Solulink (B-9007-105K; San Diego, CA, USA). A solution of biotinylated anti-fluorescein antibody (anti-FITC; 10 μg in 300 μL of saline solution) was injected through the rubber stopper of the reconstituted vial while venting the excess pressure. The vial was shaken and incubation took place for 10 min at room temperature. All prepared microbubbles were used within the same day.

The OptiCell was coated with fluorescein for the antibody to bind to anti-fluorescein in the following manner. Fluorescein-labeled bovine serum albumin (FITC-BSA) was diluted in phosphate-buffered saline (PBS, pH 7.4, GIBCO, Invitrogen, Breda, The Netherlands, 10010023) to a concentration of 0.1 mg/L. The OptiCell was filled with this solution and incubation took place overnight at room temperature. Before usage, the OptiCell was rinsed three times with PBS, then filled with 10 mL of sterile saline solution.

Method

We investigated the radial dynamics of the two different types of UCA microbubbles for a total of four different configurations. We focused on the influence of the four configurations and studied similarly-sized bubbles. We used bubbles of a size of 2 μm in radius because in our previous work (Overvelde 2010a), we had carefully investigated and fully characterized the response of phospholipid coated microbubbles of that size. The dynamics of a phospholipid-coated BG-6437 microbubble was measured far away from the wall to obtain the viscoelastic parameters of the shell (Marmottant et al. 2005) (see Fig. 1A). To investigate the influence of antibodies and the differences in the preparation protocols on the dynamics of phospholipid-coated microbubbles, the results were compared with the functionalized BG-6438 microbubbles (see Fig. 1B). In the experiment, these microbubbles were positioned 150 μm away from the wall to exclude the influence of the boundary. In the third experiment, the BG-6437 microbubble was in contact with the wall (see Fig. 1C). The results of a BG-6437 bubble at the wall and in free space were compared to confirm the influence of the boundary as discussed by Garbin et al. (2007) and Overvelde (2010a). In the previous three experiments, the bubbles were injected in an uncoated OptiCell. In the fourth experiment, the functionalized BG-6438 microbubbles adhere to the inside of an OptiCell coated with BSA-FITC solution. The schematic of this configuration is shown in Figure 1D and in the following these bubbles are referred to as adherent bubbles.

Experimental protocol

In all the experiments where the dynamics were studied in the approximation of an unbounded fluid, individual microbubbles were trapped with the optical tweezers and positioned away from the OptiCell wall. A motorized stage (M110-2.DGm; Physik Instrumente (PI), Karlsruhe, Germany) was used to accurately control the distance between the bubble in the trap and the OptiCell wall. In all experiments, the distance between the bubble and the wall was 150 μm. The laser trap was turned on during the experiments to prevent the bubbles from

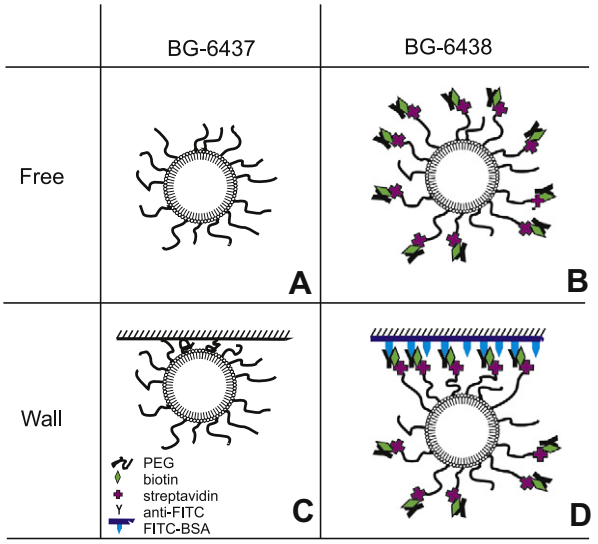

Fig. 1. Schematic drawing of the four experimental configurations. (A) Phospholipid coated microbubble away from the wall. (B) Functionalized microbubble away from the wall. (C) Phospholipid bubble floating against the OptiCell wall. (D) Functionalized microbubble adherent to the FITC-BSA coated wall. The shape and color of the markers located in the right bottom are used throughout the article for the particular configuration.

rising out of the optical focus due to buoyancy. It has been shown before that the laser trap does not influence the radial dynamics of the bubbles (Overvelde 2010a). Twelve movies of 128 frames were recorded in two runs with the Brandaris camera. The second run started after the data of the first run was transferred to the computer. The time between the two runs is of the order of 20 s and the time between two subsequent movies is 80 ms. In each experiment, a bubble was insonified with an ultrasound burst at 12 different frequencies at a constant acoustic pressure to obtain a resonance curve.

The optical tweezers were not used for the experiments on the bubbles in contact with the wall and those adherent to the wall. During these experiments, the Brandaris 128 camera was running in a segmented mode, which allowed us to record 12 movies of 64 frames in a single run. The time between two subsequent movies was 80 ms. No ultrasound was applied during the first movie. In the consecutive 11 movies, the insonation frequency was changed while the pressure was kept constant, again to recover the resonance curve of the bubble.

Resonance curves were measured based on the microbubble spectroscopy method (Van der Meer et al. 2007). The radial dynamics of the single bubble was recorded while scanning the applied frequency and keeping the applied pressure constant, which was always lower than 40 kPa. This resulted in the resonance curve of the bubble. We then repeated the experiment on the very same bubble at different acoustic pressures. As the resonance curve shifts to lower frequencies for higher acoustic pressures, the frequency range selected depends on the applied acoustic pressure. At low pressures ($P_a <$ 40 kPa), we insonify at frequencies, typically between 2 and 4 MHz. When we obtain a maximum amplitude of oscillation, we skipped the scan at the lower frequency range. Only at higher pressures ($P_a > 40$ kPa) the frequency of maximum response decreases significantly, such that we needed to investigate the lower frequency range.

Analysis

Each movie captures the radial dynamics at a single acoustic pressure and frequency. A sequence of 10 consecutive frames of an oscillating bubble is shown in Figure 2A. The radius-time curve, $R(t)$, of the bubble, $R_0 = 3.3\ \mu$m, was determined by tracking the contour of the bubble (Van der Meer et al. 2007) in each frame with a code programmed in Matlab® (The MathWorks, Inc., Natick, MA, USA), see Figure 2B. We exclude the "compression-only" behavior (De Jong et al. 2007) of an oscillating bubble by removing the low frequency component, ϵ_0 (Fig. 2C), and use the relative excursion at the fundamental frequency, A_1,

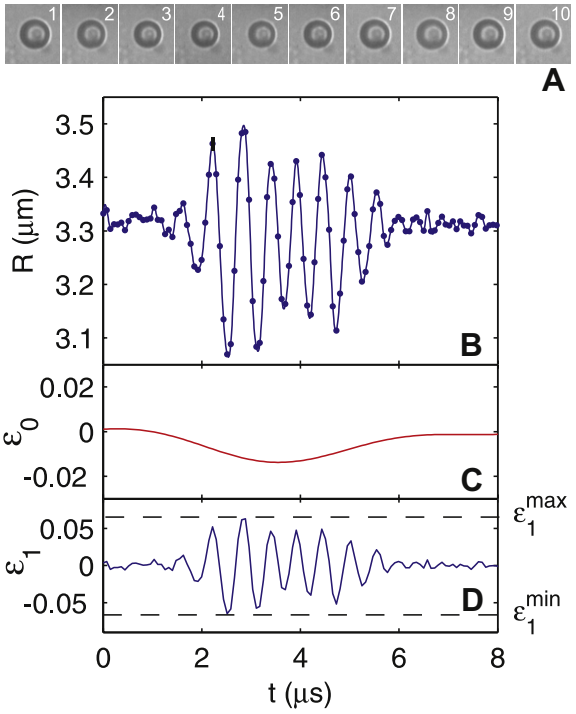

Fig. 2. (A) Frame 1-10 show a sequence of an oscillating bubble ($R_0 = 3.3\mu$m) recorded with the Brandaris 128 camera. (B) The corresponding radius-time curve. (C) The low frequency component ϵ_0. (D) The fundamental frequency component ϵ_1. The applied pressure was 17.5 kPa and the applied frequency was 1.8 MHz.

$$A_1 = \frac{\epsilon_1^{\max} - \epsilon_1^{\min}}{2}, \tag{1}$$

where $\epsilon_1^{\max}$ is the maximum relative expansion and $\epsilon_1^{\min}$ the minimum relative expansion (see Fig. 2D). Strictly speaking, the amplitude response, A_1, contains frequency components higher than the fundamental frequency. However, at the driving pressures of the experiments described here, these higher order harmonics are found to be negligible, see Sijl et al. (2011).

Throughout the article, we use the nondimensional frequency Ω to compare the results with the well-known response of an uncoated bubble:

$$\Omega = \frac{f}{f_0^{unc}} \tag{2}$$

with f the applied frequency and f_0^{unc} the eigenfrequency of the uncoated bubble (Plesset and Prosperetti 1977; Hilgenfeldt et al. 1998):

$$f_0^{unc} = \frac{1}{2\pi}\sqrt{\frac{1}{\rho R_0^2}\left(3\kappa P_0 + (3\kappa - 1)\frac{2\sigma_w}{R_0}\right)} \tag{3}$$

with $\rho = 1000$ kg/m^3 the density of the fluid, R_0 the initial bubble radius, $P_0 = 10^5$, Pa the ambient pressure, $\kappa = 1.07$

the polytropic exponent of the gas inside the bubble (Van der Meer et al. 2007), σ_w=0.072 N/m and the surface tension of the gas-liquid system. For a bubble with a radius of 2 μm, the eigenfrequency of the uncoated bubble is 1.7 MHz.

A resonance curve is obtained by plotting the relative amplitude of oscillation A_1 as a function of the applied frequency Ω (see Fig. 3). The frequency of maximum response Ω_{MR} and the maximum relative amplitude of oscillation A_1^{MR} are extracted from the resonance curves.

The shell parameters are defined with the model by Marmottant et al. (2005). The gas and liquid parameters are the same as for the uncoated bubble. The frequency of maximum response at the lowest amplitudes of oscillation is used to determine the shell elasticity χ. The value for the shell viscosity κ_s is determined from the amplitude of oscillation at the frequency of maximum response. The shell viscous damping contribution has a negligible influence on the frequency of maximum response and, while we do not know the exact value of $\sigma(R_0)$ *a priori*, in the regime of large amplitude of oscillations (A_1>0.15), the influence of the initial effective surface tension on the frequency of maximum response is ruled out (Overvelde et al. 2010b).

Errors associated with the determination of the frequency of maximum response have several sources. The error in the oscillation amplitude is estimated directly from the radius of the bubble. The optical image of the bubble is complex because of a ring pattern composed of diffraction and Mie scattering. While the error in the absolute bubble radius is on the order of 10%, (Van der Meer et al. 2007), the oscillation amplitude of the bubble is obtained from image analysis that allows for subpixel accuracy. The typical uncertainty in the radius ($R_{max}-R_{min}$) is 40 nm (Garbin et al. 2009). For a 2 μm bubble, this results in an error in the linear response, A_1, of 0.01. The error in the frequency is estimated at one half of the frequency step in the microbubble spectroscopy frequency scan, which was 0.2 MHz in the experiments described here. The error in the nondimensional frequency, Ω_{MR}, is obtained by normalizing with the resonance frequency of the uncoated bubble with a radius of 2 μm, leading to a relative error of 6%.

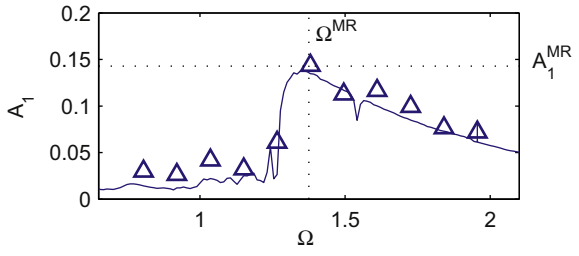

Fig. 3. Experimental resonance curve (triangles) of a BG-6437 microbubble, A_1 as a function of Ω. The bubble has a radius R_0=2 μm and is insonified with an acoustic pressure P_a=32.5 kPa. We obtain the frequency of maximum response Ω_{MR} and the maximum relative response A_1^{MR} from the resonance curve. The simulations (line) are performed with the shell buckling model (Marmottant et al. 2005). The shell parameters are a shell elasticity χ=2.5 N/m, a shell viscosity $\kappa_s=5\cdot10^{-9}$ kg/s, and an initial surface tension $\sigma(R_0)$=0.025 N/m.

RESULTS

Targeting ligands

Figure 4A shows the frequency of maximum response Ω_{MR} as a function of the maximum amplitude of oscillation A_1^{MR}. The results for a BG-6437 phospholipid-coated microbubble (blue triangles) are compared with a BG-6438 functionalized microbubble (red squares). The radius of both microbubbles is 2.0 μm and the applied pressure and frequency are scanned to cover the parameter space from P_a=15 to 45 kPa and

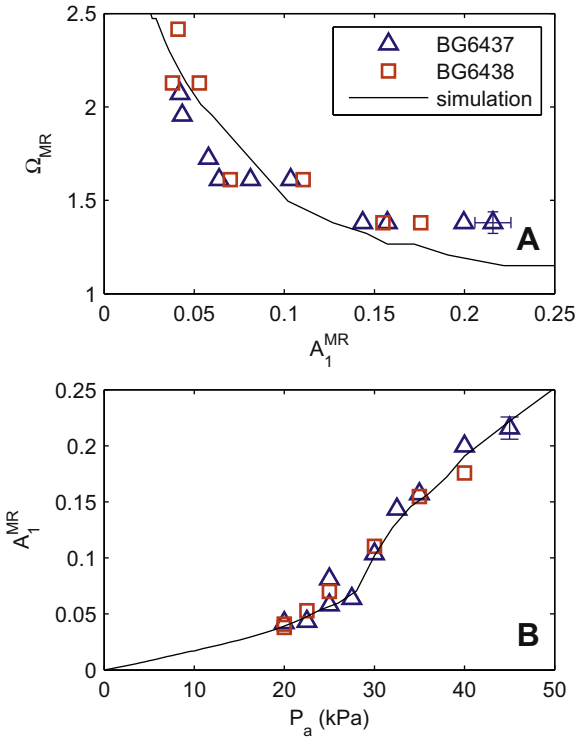

Fig. 4. Response of a phospholipid-coated microbubble (BG-6437) and a functionalized microbubble (BG-6438) in the unbounded fluid, both with a radius R_0=2 μm. The simulations are performed with the shell buckling model (Marmottant et al. 2005). The shell parameters in the simulations are χ=2.5 N/m, $\kappa_s=5\cdot10^{-9}$ kg/s and $\sigma(R_0)$=0.025 N/m. (A) The frequency of maximum response Ω_{MR} as a function of the amplitude of oscillation A_1^{MR}. (B) A_1^{MR} as a function of the applied acoustic pressure P_a.

from $f=1.2$ to 4 MHz. The bubbles are located away from the Opticell wall.

We observe a decrease in the frequency of maximum response with increasing acoustic pressure. When the maximum amplitude of oscillations is small, $A_1^{MR}<0.05$, the frequency of maximum response is large, $\Omega_{MR}\geq 2$. For larger amplitude of oscillation, $A_1^{MR}>0.15$, the frequency of maximum response tends to converge to $\Omega_{MR}=1.3$. We observe a similar decrease of the frequency of maximum response with increasing pressure for BG-6437 and BG-6438 bubbles. Furthermore, the trend corresponds with the behavior of the phospholipid-coated agent BR-14 initially oscillating in the elastic regime. We compare the experimental results with the model developed for coated bubbles for large amplitude oscillations by Marmottant et al. (2005) in the configuration as used by Overvelde et al. (2010b).

The simulations with the shell-buckling model of Marmottant et al. (2005) are depicted in Figure 4A with the shell parameters $\chi=2.5$ N/m, $\kappa_s=5\cdot 10^{-9}$ kg/s and $\sigma(R_0)=0.025$ N/m. The simulations and experiments are in very good agreement up to an amplitude $A_1^{MR}=0.15$. For $A_1^{MR}>0.15$, a small deviation is encountered: the simulation systematically underestimates the resonance frequency by a small but significant amount.

The relative amplitude of oscillation at A_1^{MR} as a function of the driving pressure P_a is shown in Figure 4B. The smallest oscillations are observed at an acoustic pressure $P_a=20$ kPa. The increase of the maximum amplitude of oscillation with the acoustic pressure is very similar for phospholipid-coated microbubbles and functionalized microbubbles. The nonlinear increase of the amplitude A_1^{MR} with pressure is in excellent agreement with the prediction of the shell-buckling model (Marmottant et al. 2005). The shell parameters are comparable to the values used for BR-14 microbubbles. We conclude that the ligands do not seem to influence the frequency of maximum response and the maximum amplitude of oscillation of phospholipid-coated microbubbles.

Proximity of the wall

Figure 5A shows the frequency of maximum response as a function of the amplitude A_1^{MR} for a phospholipid-coated bubble $R_0=2$ μm at a distance of 150 μm away from the wall (blue triangles) and for a phospholipid-coated microbubble $R_0=2.1$ μm in contact with the wall (green circles). The dynamics of the bubble away from the wall are investigated by scanning the frequency between 1.2 and 4.2 MHz and the pressure between 20 and 45 kPa. The bubble in contact with the wall is insonified with a frequency between 1 and 4.8 MHz and an applied pressure between 30 and 100 kPa. The influence of the wall on the frequency of maximum response is most noticeable at an amplitude

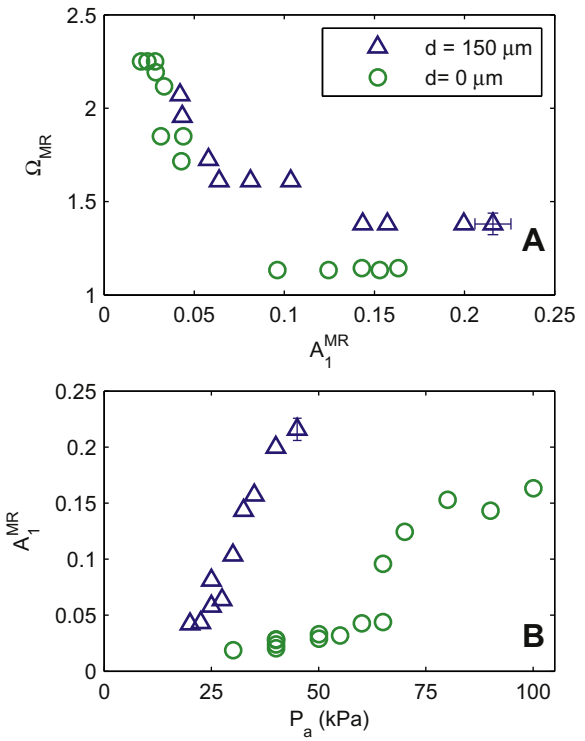

Fig. 5. Response of a phospholipid-coated microbubble (BG-6437) with a radius $R_0=2$ μm far away from the wall ($d_{wall}=150$ μm, blue triangles) and the response of a BG-6437 bubble with a radius $R_0=2.1$ μm at the wall ($d_{wall}=0$ μm, green circles). (A) The frequency of maximum response Ω_{MR} as a function of the amplitude of oscillation A_1^{MR}. (B) A_1^{MR} as a function of the applied acoustic pressure P_a.

$A_1^{MR}>0.15$, where Ω_{MR} reaches an almost constant value. This "plateau" is reached for the bubble in free space at $\Omega_{MR}=1.3$ and for the bubble at the wall the frequency of maximum response is 20% lower $\Omega_{MR}=1.1$. Figure 5B shows the amplitude of oscillation A_1^{MR} at Ω_{MR} as a function of P_a for both cases: at the wall and away from the wall. The maximum amplitude of oscillation A_1^{MR} of the bubble in free space increases rapidly with increasing pressure, reaching an amplitude $A_1^{MR}=0.15$ at a pressure $P_a=37.5$ kPa, while the bubble at the wall reaches the same amplitude of oscillation only for a much higher pressure $P_a=80$ kPa.

Adherence to the wall

The response of the bubble A_1 is shown in the iso-contour plot in Figure 6 for the full set of applied pressures and frequencies. The response of a phospholipid-coated microbubble with a radius $R_0=2.1$ μm at the wall (A) is compared with the response of a microbubble with similar radius $R_0=2.2$ μm adherent to the wall (B). As observed in Figure 5A, the frequency of maximum response Ω_{MR} of the bubble in contact with the wall

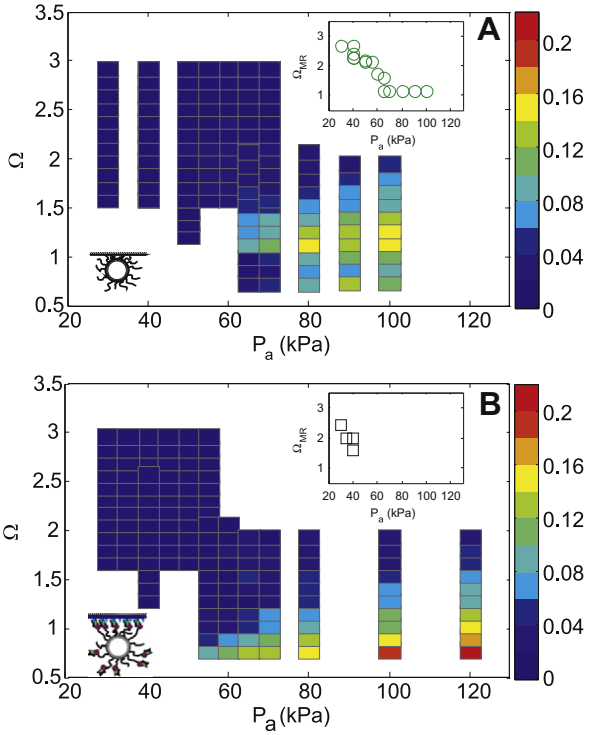

Fig. 6. The relative amplitude of oscillation A_1 as a function of the acoustic pressure P_a and frequency Ω. The frequency of maximum response as a function of the acoustic pressure is shown in the inset. (A) The response of a bubble $R_0=2.1$ μm in contact with the wall. (B) The response of a bubble $R_0=2.2$ μm adherent to the wall.

decreases with increasing pressure as shown in the inset of Figure 6A, reaching a frequency $\Omega_{MR}=1.1$ at a pressure $P_a \geq 65$ kPa. However, for the bubble floating up against the wall, a second peak appears at the lowest applied frequency at acoustic pressures of 80 kPa and higher (see also Fig. 7). For the bubble adherent to the wall (Fig. 6B), the highest response is observed at the lowest applied frequency $\Omega=0.7$ at acoustic pressures $P_a \geq 55$ kPa. The frequency of maximum response could, therefore, only be obtained at the low applied acoustic pressures (see inset of Fig. 6B). Unfortunately, due to the limited bandwidth of the transducer, the bubbles could not be investigated at even lower frequencies to reveal the frequency of maximum response of the targeted bubble and the origin of the second peak.

The resonance curves of the bubble in contact with the wall and those of the adherent bubble shown in Figure 6 are compared in Figure 7 at an acoustic pressure of 100 kPa. We observe that the amplitude of oscillation of the adherent bubble at $\Omega=0.7$ (which, as already indicated above, is not its frequency of maximum response) is already 25% higher than the amplitude A_1^{MR} of the bubble at the wall. Comparing the frequency of maximum response of the adherent bubble $\Omega_{MR} \leq 0.7$ with the

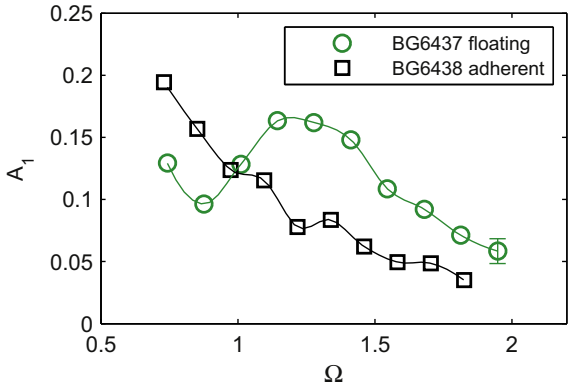

Fig. 7. Resonance curve of a phospholipid-coated bubble (BG-6437) in contact with the wall (green circles) and a functionalized bubble (BG-6438) adherent to the wall (black diamonds) insonified with a pressure $P_a=100$ kPa. The resonance curves are obtained from Figure 6.

bubble in the unbounded fluid $\Omega_{MR}=1.4$, a decrease is observed of at least 50%. To ensure that there was no contribution to the change in resonance frequency due to the vicinity of other bubbles, we considered the effect of the closest bubble in the field of view (distance $7R_0$). In this case, simulations with the Marmottant model for a coated bubble as used above, but now for a bubble near a rigid wall, show that the neighboring bubble decreases the frequency of maximum response with only 8% and, consequently, it cannot account for the 50% change in response.

DISCUSSION

In all experiments, we operate the system in a regime of large amplitude of oscillation, A_1. With $A_1>0.15$, the frequency of maximum response is hardly affected by the initial properties of the coating (Overvelde 2010a) and only the influence of the neighboring wall and adherence to the wall is investigated. We observe no influence of the targeting ligands on the dynamics of bubbles away from the wall, hence, no influence of the preparation protocol is expected on the behavior of the bubbles. Previous studies have shown a difference in dynamics between adherent and free bubbles. Zhao et al. (2006) showed that the oscillation amplitude and the frequency response of adherent bubbles are different from those of freely floating bubbles. However, in the same experiment bubbles do cluster, which may in part lead to the change in the observed response. Zhang et al. (2007) show that they can in fact distinguish acoustically between adherent and freely floating bubbles. In this article, we combine in an unique set-up the ultra high speed camera with optical tweezers to allow for a detailed study of the resonance frequency of single bubbles, both freely floating and in contact with and adherent to the wall. We quantified the

decrease of the frequency of maximum response for a bubble adherent to a wall with respect to a bubble in free space and floating against a wall.

We may attempt to interpret the observed change in response by drawing the analogy with a harmonic oscillator model (see *e.g.*, Plesset and Prosperetti 1977). An oscillating bubble can be thought of as a mass-spring system where the inertia ("mass" m of the oscillator) is due to the surrounding fluid being displaced, and the restoring force (with "spring" stiffness k) comes from the gas inside the bubble being compressed. For a coated bubble, the viscoelastic coating also contributes to the stiffness of the system. The interaction of a bubble with a perfectly rigid wall can be modeled through the method of images (see *e.g.*, Leighton 1994) where the wall is replaced by an "image" bubble oscillating in phase with the same amplitude and phase as the real bubble. This effectively results in an increased inertia of the system and, therefore, in a decrease of the eigenfrequency $\omega_0=\sqrt{k/m}$ of approximately 20%. The much larger decrease of the frequency of maximum response for a bubble adherent to a wall can be interpreted as a much larger decrease in k/m. On the other hand, the OptiCell wall is compliant and cannot simply be modeled by a rigid wall model with an identical bubble oscillating in phase (Allen et al. 2003; Overvelde 2010a). In particular, longitudinal modes of oscillations can be excited in a thin compliant wall. Furthermore, the fact that the bubble is adherent to the wall can produce a more efficient coupling of the dynamics of the bubble and the wall. This coupling can cause a change in the total k/m and possibly a change in the total damping. However, at this stage we are not able to rule out mechanism that causes the decrease in the frequency of maximum response and quantitatively predict its magnitude.

CONCLUSIONS

In conclusion, we investigated the influence of adhesion of a functionalized bubble to a target membrane on its frequency of maximum response and amplitude of oscillation. The bubble dynamics in the unbounded fluid was found to be unchanged for bubbles containing targeting ligands compared with phospholipid-coated microbubbles alone. A comparison of the response of a functionalized bubble in the unbounded fluid with the response of an adherent bubble resulted in a decrease of over 50% of the frequency of maximum response for the adherent microbubble. The frequency of maximum response of a phospholipid-coated bubble floating up against an OptiCell wall was observed to decrease by only 20%, which is in excellent agreement with previously obtained results for bubble-wall interactions (Overvelde 2010a). This finding may prove useful for developing imaging protocols to discriminate between adherent and freely circulating bubbles.

Acknowledgments—The authors thank Peter Frinking and Thierry Bettinger from Bracco Research S.A. (Geneva, Switzerland) for discussions and for supplying the contrast agents. The authors thank Nenad Gajovic-Eichelman of the Fraunhofer Institute for the anti-fluorescein antibody and FITC-labeled BSA and Klazina Kooiman for fruitful discussions, help and practical information on the targeting of microbubbles. This work was partly financed by TAMIRUT, a Specific Targeted Research (STReP) project supported by the 6th Framework Programme of the European Commission in the Nanosciences, Nanotechnologies, Materials and new Production Technologies area under contract number NMP4-CT-2005-016382.

REFERENCES

Allen JS, Kruse DE, Dustin E, Dayton PA, Ferrara KW. Effect of coupled oscillations on microbubble behavior. J Acoust Soc Am 2003;114:1678.

Chin CT, Lancée C, Borsboom J, Mastik F, Frijlink ME, De Jong N, Versluis M, Lohse D. Brandaris 128: A digital 25 million frames per second camera with 128 highly sensitive frames. Rev Sci Instr 2003;74:5026–5034.

Dayton PA, Allen JS, Ferrara KW. The magnitude of radiation force on ultrasound contrast agents. J Acoust Soc Am 2002;112:2183–2192.

Dayton PA, Klibanov AL, Brandenburger G, Ferrara KW. Acoustic radiation force *in vivo*: A mechanism to assist targeting of microbubbles. Ultrasound Med Biol 1999;25:1195–1201.

Doinikov AA, Zhao S, Dayton PA. Modeling of the acoustic response from contrast agent microbubbles near a rigid wall. Ultrasonics 2009;49:195–201.

Eniola AO, Willcox PJ, Hammer DA. Interplay between rolling and firm adhesion elucidated with a cell-free system engineered with two distinct receptor-ligand pairs. Biophys J 2003;85:2720–2731.

Garbin V, Cojoc D, Ferrari E, Di Fabrizio E, Overvelde MLJ, Van der Meer SM, De Jong N, Lohse D, Versluis M. Changes in microbubble dynamics near a boundary revealed by combined optical micromanipulation and high-speed imaging. Appl Phys Lett 2007;90:114103.

Garbin V, Dollet B, Overvelde M, Cojoc D, Di Fabrizio E, Wijngaarden L, Prosperetti A, de Jong N, Lohse D, Versluis M. History force on coated microbubbles propelled by ultrasound. Phys Fluids 2009;21:092003.

Ham AS, Klibanov AL, Lawrence MB. Action at a distance: Lengthening adhesion bonds with poly(ethylene glycol) spacers enhances mechanically stressed affinity for improved vascular targeting of microparticles. Langmuir 2009;25:10038–10044.

Hilgenfeldt S, Lohse D, Zomack M. Response of bubbles to diagnostic ultrasound: A unifying theoretical approach. Eur Phys J B 1998;4:247–255.

De Jong N, Emmer M, Chin CT, Bouakaz A, Mastik F, Lohse D, Versluis M. "Compression-Only" behavior of phospholipid-coated contrast bubbles. Ultrasound Med Biol 2007;33:653–656.

Klibanov AL. Preparation of targeted microbubbles: Ultrasound contrast agents for molecular imaging. Med Biol Eng Comput 2009;47:875–882.

Klibanov AL, Rychak JJ, Yang WC, Alikhani B, Acton S, Lindner JR, Ley K, Kaul S. Targeted ultrasound contrast agent for molecular imaging of inflammation in high-shear flow. Mol Imaging 2006;266:259–266.

Lankford M, Behm CZ, Yeh J, Klibanov AL, Robinson P, Lindner JR. Effect of microbubble ligation to cells on ultrasound signal enhancement. implications for targeted imaging. Invest Radiol 2006;41.

Leighton TG. The acoustic bubble. San Diego, CA: Academic Press; 1994.

Lindner JR. Microbubbles in medical imaging: Current applications and future directions. Nat Rev Drug Discov 2004;3:527–533.

Marmottant P, Van der Meer SM, Emmer M, Versluis M, De Jong N, Hilgenfeldt S, Lohse D. A model for large amplitude oscillations

of coated bubbles accounting for buckling and rupture. J Acoust Soc Am 2005;118:3499–3505.
Overvelde M. Ultrasound contrast agents: Dynamics of coated bubbles. Ph.D. thesis. 2010a.
Overvelde M, Garbin V, Sijl J, de Jong N, Lohse D, Versluis M. Nonlinear shell behavior of phospholipid-coated microbubbles. Ultrasound Med Biol 2010b;36:2080–2092.
Plesset MS, Prosperetti A. Cavitation and bubble dynamics. Ann Rev Fluid Mech 1977;9:145–185.
Rychak JJ, Klibanov AL, Ley KF, Hossack JA. Enhanced targeting of ultrasound contrast agents using acoustic radiation force. Ultrasound Med Biol 2007;33:1132–1139.
Sijl J, Overvelde M, Dollet B, Garbin V, de Jong N, Lohse D, Versluis M. 'Compression-only' behavior: A second order nonlinear response of ultrasound contrast agent microbubbles. J Acoust Soc Am 2011;129: 1729–1739.
Schneider M, Bichon D, Bussat P, Puginier J, Hybl, E. Patent WO 91/ 15244. 1991.
Takalkar AM, Klibanov AL, Rychak JJ, Lindner JR, Ley K. Binding and detachment dynamics of microbubbles targeted to P-selectin under controlled shear flow. J Control Rel 2004;96:473–482.
Van der Meer SM, Dollet B, Chin CT, Bouakaz A, Voormolen M, De Jong N, Versluis M, Lohse D. Microbubble spectroscopy of ultrasound contrast agents. J Acoust Soc Am 2007;121: 648–656.
Zhang D, Gong Y, Gong X, Liu Z, Tan K, Zheng H. Enhancement of subharmonic emission from encapsulated microbubbles by using a chirp excitation technique. Phys Med Biol 2007;52: 5531–5544.
Zhao S, Kruse DE, Ferrara KW, Dayton PA. Acoustic response from adherent targeted contrast agents. J Acoust Soc Am 2006;120: EL63–EL69.